Enabling Vehicular mmWave Communication Links using cmWave Information

Markus Hofer*, Faruk Pasic†, Benjamin Rainer*, Jiri Blumenstein⊕, Ales Prokes⊕,
Christoph F. Mecklenbräuker†, Andreas F. Molisch‡ and Thomas Zemen*

*AIT Austrian Institute of Technology GmbH, Austria
†Institute of Telecommunications, TU Wien, Vienna, Austria
⊕Dept. of Radio Electronics, Brno University of Technology, Czech Republic
‡University of Southern California, Los Angeles, CA, USA

***Abstract*—Future connected cooperative automated mobility can benefit from high-data-rate wireless communication links between vehicles to exchange LIDAR and/or RADAR data. The millimeter wave (mmWave) frequency range offers large bandwidth for rapid sensor data exchange but suffers from higher signal attenuation compared to the centimeter wave (cmWave) band. In this paper we obtain cmWave and mmWave multipath component (MPC) parameters by combining a single omni-directional antenna that is used as virtual array with the CLEAN algorithm. The cmWave MPC information enables low-overhead mmWave beamforming by means of an antenna array. Empirical multi-band measurement data (3.2 GHz, 34.3 GHz, and 62.35 GHz) shows that considering the 5 strongest MPCs, a signal-to-noise ratio of up to 25 dB for a V2I scenario can be achieved.**

***Index Terms*—out-of-band, mmWave, CLEAN, virtual antenna array, software defined radio**

I. Introduction

Reliable vehicular millimeter wave (mmWave) communication links are an important component for fast LIDAR and/or RADAR data exchange to provide the foundation for connected cooperative automated mobility (CCAM). The mmWave frequency band (24 GHz – 300 GHz) offers wide bandwidth, while the signal attenuation is substantially increased compared to the centimeter wave (cmWave) band (0 to 7 GHz) [1]. The cmWave band has favorable propagation conditions but offers only small available bandwidth, due to spectrum shortage.

A promising approach for reducing the overhead in mmWave link establishment is utilizing channel state information (CSI) from the cmWave band [2]. Such out-of-band information shall aid and possibly improve the link configuration in the mmWave band [3]. So far, several strategies that leverage out-of-band information have been proposed. In [4], the authors propose a compressed beam-selection approach utilizing spatial information obtained at cmWave to aid configuring the mmWave link in static scenarios. The authors of [5] propose non-parametric and parametric approaches to translate the cmWave spatial correlation to the mmWave band. Furthermore, the authors of [6] use the cmWave channel covariance as an out-of-band side information for mmWave link configuration. Sim et al. [7] have proposed a deep learning-based beam selection algorithm exploiting cmWave side information, and validated it with 3D ray-tracing simulations and over-the-air experiments. The authors of [8] develop an efficient deep-learning model to predict blockages at mmWave using cmWave information and [9] propose a beam direction-based metric to assess the power loss and the number of false directions if out-of-band spatial information is used instead of in-band information. In [10], the authors propose estimating CSI in mmWave multiple-input multiple-output (MIMO) systems leveraging out-of-band information from a cmWave MIMO system in a static line-of-sight (LOS) scenario. The proposed approach relies on joint angle of arrival (AoA)/angle-of-departure (AoD) estimation for the free-space LOS component only. Finally, the authors of [11] investigate multi-band assisted beam steering in an industrial scenario and show that beam steering in the mmWave band, using information from the cmWave band, outperforms position sensor based beam steering.

The results of all these aforementioned works show that the beam training overhead in mmWave can be reduced substantially if cmWave information is used, but only if the propagation channels at different frequency bands share a sufficient degree of similarity. In [12], strong similarities between cmWave and mmWave for an urban vehicular scenario have been shown using empirical multi-band measurement data.

Contribution of the paper:

- We combine the CLEAN algorithm [12] and a single omni-directional antenna in the cmWave band, used as virtual antenna array [1], to extract multipath component (MPC) parameters. This information enables low-overhead mmWave channel estimation and beamforming by means of an antenna array. Compared to [10], no MIMO antenna array in the cmWave band is required, and a mobile vehicular scenario is considered.
- We analyze the achieved signal-to-noise ratio (SNR) in the mmWave band per stationarity region and show that in LOS, a sufficiently large SNR can be achieved using the detected MPCs from the cmWave band.

II. Vehicular Multi-Band Communication Concept

We consider a multi-band communication link in a mobile scenario, where cmWave and mmWave communication links operate simultaneously. The cmWave link is utilized for low-data-rate exchange, while the mmWave link is reserved for high-data-rate transmission, such as LIDAR and/or RADAR data exchange.

In the proposed vehicular scenario the transmitter (TX) is moving with velocity v alongside a trajectory. Both the TX and receiver (RX) are equipped with omni-directional antennas for the cmWave band and a directional antenna for the mmWave band to mitigate the higher path loss. The directional antenna can be implemented using either a MIMO antenna array or a (steerable) directional horn antenna, as used for the measurement setup described in Sec. V. In our setup, the antennas for the cmWave and mmWave band are collocated on both the TX and RX side. The higher the path loss, the more antenna elements are required for the mmWave antenna array, resulting in narrow beams. To accelerate beam search and link establishment in the mmWave band, we leverage AoA information obtained from the cmWave band.

Using the reciprocity principle, the moving omni-directional TX antenna can be considered as a virtual antenna array [1]. We use the channel transfer function (CTF) sequence obtained within a stationarity region [13], [14] and apply the CLEAN algorithm [12], [15] to obtain estimates on path weight, Doppler shift and delay of the MPCs. With that information, the strongest MPCs and their AoA can be identified in the cmWave band and used for beamforming in the mmWave band.

Organization: In Section III we present the used radio channel model and in Section IV the parameter evaluation. The collection of the empirical measurement data is described in Sec. V. and the obtained results are described in Sec. VI.

III. Radio Channel Model

We represent the time-variant CTF within stationarity region s with length M in time and width Q in frequency as sum of P MPCs

$$H_{s,f}[m,q] = H_{\mathrm{TX}}[q] H_{\mathrm{RX}}[q] \sum_{p=1}^{P} \alpha_{s,p,f} \mathrm{e}^{\mathrm{j}2\pi(\theta_{s,p,f} m - \nu_{s,p,f} q)} , \tag{1}$$

where $\alpha_{s,p,f} \in \mathbb{C}$ is the complex path coefficient, $\nu_{s,p,f}$ is the normalized Doppler shift, $\theta_{s,p,f}$ is the normalized delay of the p-th MPC and f denotes the center frequency. Discrete time, sampled with sampling time T_{S}, is denoted by $m \in \{0, \ldots, M-1\}$, and discrete frequency, with frequency spacing $B_{\mathrm{S}} = B/Q$ is denoted by $q \in \{-Q/2, \ldots, Q/2-1\}$, where B denotes bandwidth. We assume that within the stationarity regions $[m,q] \in [0, \ldots, M] \times [-Q/2, \ldots, Q/2]$ the statistics of the fading process do not change significantly. Absolute time $m' = sM + m$. The frequency responses of TX and RX are denoted by H_{TX} and H_{RX}, respectively.

IV. Parameter Estimation

Using the CLEAN algorithm [12], [15] we estimate the MPC parameters $(\hat{\alpha}_{s,p,f}, \hat{\nu}_{s,p,f}, \hat{\theta}_{s,p,f})$ of the first $P' < P$ strongest paths within each stationarity region and for each frequency band $f \in \{f_{\mathrm{cm}}, f_{\mathrm{mm}}\}$. The CLEAN algorithm computes the scattering function for the stationarity region s, and identifies the strongest component in the delay-Doppler domain. Next, a high resolution search on a grid is performed around the strongest component to identify the real valued delay and Doppler of the MPC, and its weight is estimated. Finally, the newly identified MPC is subtracted from the scattering function and the CLEAN algorithm continues until P' MPCs are identified. A particular application of the CLEAN algorithm for a vehicular multi-band measurement scenario is shown in [12].

We can represent the time-variant frequency response as

$$H_{s,f}[m,q] = H_{\mathrm{TX}}[q] H_{\mathrm{RX}}[q] \left(H'_{s,f}[m,q] + R'_{s,f}[m,q] \right) , \tag{2}$$

with

$$H'_{s,f}[m,q] = \sum_{p=1}^{P'} \hat{\alpha}_{s,p,f} \mathrm{e}^{\mathrm{j}2\pi(\hat{\theta}_{s,p,f} m - \hat{\nu}_{s,p,f} q)} , \tag{3}$$

where $R'_{s,f}[m,q]$ denotes the residual that is not represented by the first P' strongest MPCs.

A. Angle-of-Arrival Estimation

The normalized Doppler shift of a single MPC can be expressed by the velocity v_s of the vehicle within stationarity region s by

$$\hat{\nu}_{s,p,f} = \frac{v_s}{c_0} f T_{\mathrm{S}} \cos(\hat{\phi}_{s,p,f}) . \tag{4}$$

Hence, we can estimate the AoA $\hat{\phi}_{s,p,f}$ by

$$\hat{\phi}_{s,p,f} = \arccos\left(\frac{\hat{\nu}_{s,p,f}}{f T_{\mathrm{S}}} \frac{c_0}{v_s} \right) , \tag{5}$$

where $\hat{\nu}_{s,p,f}$ is the normalized Doppler shift of the p-th MPC and c_0 is the speed of light. Please note that this estimation has a 180° degree ambiguity. For evaluation, stationarity regions with sufficiently large velocity v_s are taken into account. We further assume that the velocity is known at the receiver and time division duplex communication is used. The AoA estimation is performed for all frequency bands $f \in \{f_{\mathrm{cm}}, f_{\mathrm{mm}}\}$.

B. AoA Matching

To investigate whether MPCs with similar AoAs occur in the cmWave and in the mmWave band, we assume that the MPCs at the mmWave band are received within the angular interval

$$\mathcal{D}_{s,p,f_{\mathrm{cm}}} = (\hat{\phi}_{s,p,f_{\mathrm{cm}}} - \beta/2,\ \hat{\phi}_{s,p,f_{\mathrm{cm}}} + \beta/2), \tag{6}$$

where β denotes the utilized opening angle. We assume that the CLEAN algorithm consistently estimates the center of the arriving MPC, such that we can set the angular bounds as defined in (6). We use the following algorithm per stationarity

region to match the MPCs in the mmWave band to the strongest MPC in the cmWave band:

- In each band, sort the MPCs according to magnitude $|\hat{\alpha}_{s,p,f}|$ and consider the first $P' < P$ strongest paths.
- Choose the strongest MPC, $p = 1$, from f_{cm} and check how many MPCs in the mmWave band are within the opening angle interval of the cmWave band, i.e., find all MPCs for f_{mm}, $p' \in \{1, \ldots, P'\}$ where

$$\hat{\phi}_{s,p',f_{\text{mm}}} \in \mathcal{D}_{s,p,f_{\text{cm}}}$$

  and create set $\mathcal{P}_s$ containing all these p'.

If $|\mathcal{P}_s| > 0$, we observe MPCs in the mmWave band with the same AoAs as in the cmWave band. Hence, the AoA $\hat{\phi}_{s,p,f_{\text{cm}}}$ can be used for analog beamforming in the mmWave band to improve the SNR. For digital beamforming an MPC matching algorithm can be applied, which takes both, the delay and the Doppler shift into account, while maximizing the SNR.

C. Signal-to-Noise Ratio

With the set $\mathcal{P}_s$ we calculate the SNR of the mmWave band per stationarity region according to

$$\text{SNR}_{s,f_{\text{mm}}} = \frac{\sum_{p' \in \mathcal{P}_s} |\hat{\alpha}_{s,p',f_{\text{mm}}}|^2}{\sigma^2_{s,f_{\text{mm}}}} \tag{7}$$

where $\sigma^2_{s,f_{\text{mm}}}$ is the noise level in the mmWave band, estimated from the time-variant channel impulse response in each stationarity region.

D. Residual Energy

To assess how much energy is captured with the strongest MPCs, we define the normalized residual energy within a stationarity region

$$\gamma_{s,f} = \frac{\sum_{m=0}^{M-1} \sum_{q=-Q/2}^{Q/2-1} |R'_{s,f}[m,q]|^2}{\sum_{m=0}^{M-1} \sum_{q=-Q/2}^{Q/2-1} |H_{s,f}[m,q]|^2}, \tag{8}$$

where $H_{s,f}[m,q]$ and $R'_{s,f}[m,q]$ are given in (2). The larger the energy captured by the first MPCs, the smaller $\gamma_{s,f}$.

V. Measurement Description

As a proof of concept, we demonstrate that the AoAs in both cmWave and mmWave bands are comparable using multi-band channel sounding measurements from an urban street scenario near the AIT in Giefinggasse, 1210 Vienna, Austria.

We apply the algorithm shown in Section IV-B to the time-variant CTFs obtained by a triple-band (3.2 GHz (cmWave), 34.3 GHz (mmWave band 1) and 62.35 GHz (mmWave band 2)) channel measurement campaign [16] conducted in an urban vehicle-to-infrastructure (V2I) street scenario shown in Fig. 1. Note that, in this setup we apply the algorithm to the combinations cmWave-mmWave band 1 and cmWave-mmWave band 2 separately. A TX car, equipped with three omni-directional antennas covering three frequency bands, is traveling along the indicated trajectory on an urban street towards a road intersection. A real time kinematic global positioning system (GPS) system is used to track the position

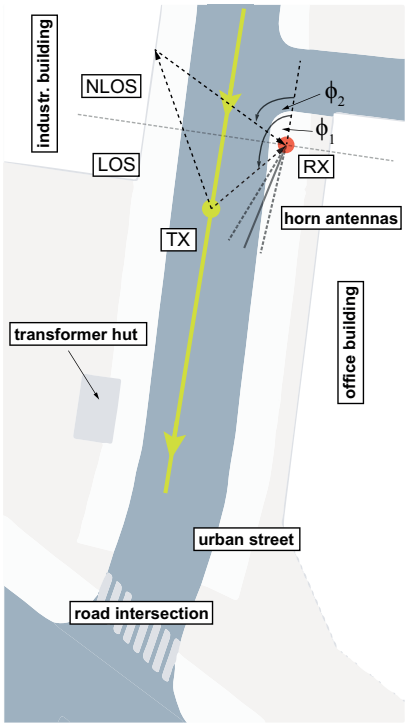

Fig. 1. Overview of the measurement scenario [16]. A TX car approaches a road intersection and stops. The directive RX horn antennas are pointed towards the road intersection. Indicated are a direct MPC from TX to RX (ϕ_1) as well a reflection via an industrial building (ϕ_2).

and velocity of the TX. The RX is positioned approximately 1.5 meters above street level, next to an office building. It is equipped with three vertically aligned directional antennas. Each antenna has a similar half power beam width (HPBW) of 18° and they are oriented towards the road intersection. The channel measurement lasts for 30 seconds, during which the TX passes by the RX at 11.6 seconds and comes to a stop at the road intersection at 21 seconds. For time and frequency synchronization Rubidium clocks are utilized. At the receiver the time-variant CTFs are recorded every $t_{\text{R}} = 31.25\,\mu\text{s}$ for all frequency bands simultaneously and stored on a hard disk. The measurement parameters used in this measurement are provided in Tab. I. More details of the measurement scenario can be found in [16].

Please note that the antenna configuration of this measurement at the RX is a proof of concept setup with directional antennas in the cmWave and mmWave band, which are already pointing in the same direction. Hence, the AoA matching algorithm in IV-B will obtain good AoA matches specifically in the HPBW of the antennas.

VI. Results

We evaluate the recorded CTFs between the times 11.6 s and 15 s of the measurement, which corresponds to the LOS interval of the measurement. We choose a stationarity region length with $T_{\text{stat}} = 100\,\text{ms}$ which is equal to $M = 3200$ time samples. We set the number of considered MPCs to $P' = 5$ and $\beta = 18°$. In the following subsections we evaluate, the residual energy, the AoAs of the detected MPCs and the SNR.

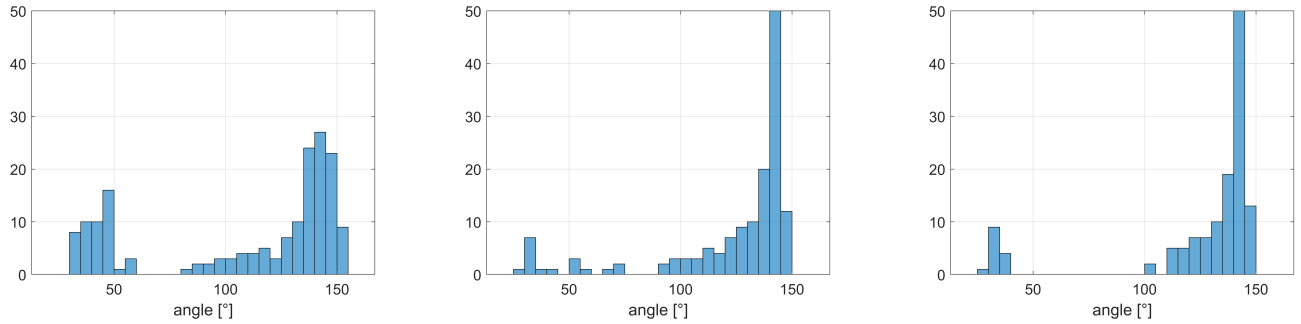

(a) AoA histogram of MPCs at 3.2 GHz. (b) AoA histogram of MPCs at 34.3 GHz. (c) AoA histogram of MPCs at 62.35 GHz.

Fig. 2. AoA histograms of the fist $P' = 5$ MPCs during the time-interval $(11.6\,\mathrm{s}, 15\,\mathrm{s})$ at the frequency bands 3.2 GHz, 34.3 GHz and 62.35 GHz

TABLE I
CHANNEL SOUNDING PARAMETERS

Parameter	Value
Carrier frequency f_c	3.2, 34.3, 62.35 GHz
Number of subcarriers Q	311
Subcarrier spacing $\triangle f$	500 kHz
Bandwidth B	155.5 MHz
Symbol duration t_s	2 µs
Interval between snapshots t_R	31.25 µs
Measurement duration t_m	30 s
Max. relative velocity v_{max}	1500, 140, 77 m/s

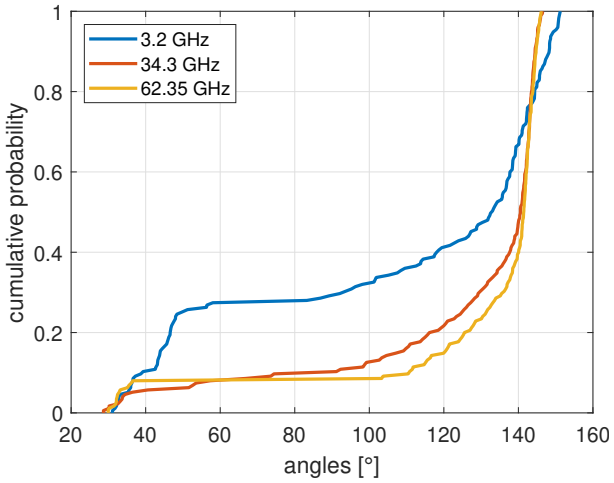

Fig. 3. Empirically calculated AoA CDF of the first $P' = 5$ MPCs within 11.6 s to 15 s for all bands.

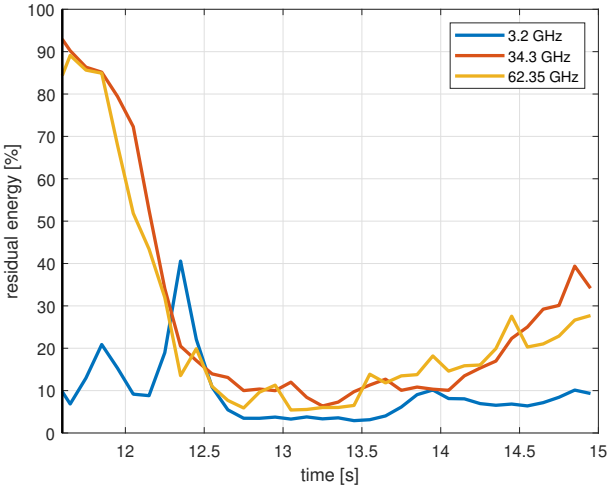

Fig. 4. Residual energy in percentage vs. time within the interval $(11.6\,\mathrm{s}, 15\,\mathrm{s})$ for the 3.2 GHz, 34.3 GHz and 62.35 GHz band.

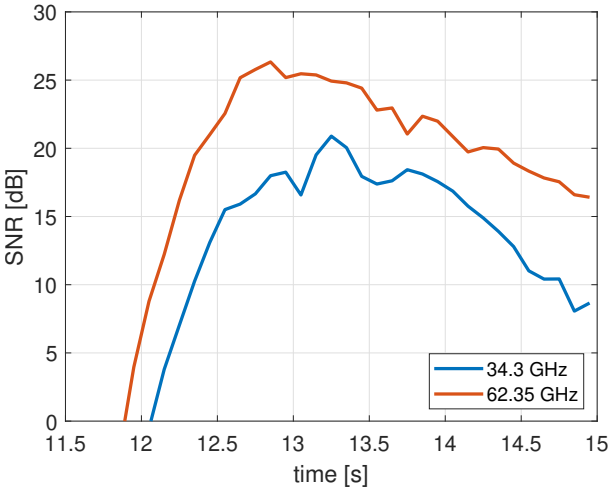

Fig. 5. SNR (c.f. (7)) for the mmWave bands vs. time within the interval $(11.6\,\mathrm{s}, 15\,\mathrm{s})$ for the 34.3 GHz and 62.35 GHz.

A. Residual Energy

In Fig. 4 we show the residual energy (c.f. (8)) in each stationarity region vs. time within each frequency band after the detection of the first P' strongest MPCs. We observe, that with the considered setup, as soon as the TX moves within the HPBW of the directional receive antenna, a comparably large portion of the energy is detected by the strongest MPCs in all frequency bands.

B. AoA Statistics

We statistically analyze the AoAs obtained by (5) for each frequency band and plot their histograms for the defined evaluation time (11.6 to 15 s) in Fig. 2. The empirically calculated CDFs are shown in Fig. 3. The results for this measurement show essentially two AoA clusters. The first AoA cluster is between 20 – 40° (corresponding to reflected MPCs) and shows fewer detected MPCs especially in the mmWave band. The second AoA cluster is around 120 – 140° and corresponds to direct MPCs. It can be further observed that for both bands, cmWave and mmWave, a large amount of AoAs falls into this cluster. This can be explained by the antenna pattern of the directive antennas used both in the cmWave and mmWave bands. We expect that if omni-directional antennas are used in the cmWave band a higher amount of reflected MPCs will be observed. Since there is strong similarity between cmWave and mmWave bands (specifically if the directional antennas point in the same direction), we expect that these MPCs also exist in the mmWave band (especially for specular reflections), offering an alternative communication link in the mmWave band.

C. Signal-to-Noise Ratio

We finally assess the link quality by calculating the SNR over time using (7) in Section IV-C. The results are shown in Fig. 5. We observe, that, with the proposed AoA matching algorithm the SNR achieved in the mmWave band, using the strongest detected MPC in the cmWave, is sufficiently large for high data rate transmission. Please note, that in this specific setup, the SNR at the 62.35 GHz band is higher due to the higher transmit power used in that band.

VII. Conclusions

In this paper we provide a proof of concept to enable communication link establishment in the mmWave frequency band using AoA information from the cmWave frequency band. We obtain the AoAs from MPC parameters estimated by the CLEAN algorithm using the virtual antenna array principle. Subsequently, we define an AoA matching algorithm that searches for MPCs within a similar opening angle in the cmWave and mmWave band. Finally, we apply the defined algorithm to a triple band measurement from an urban scenario. The results show that specifically for the LOS case mmWave communication links with sufficiently large enough SNR can be achieved.

Acknowledgement

This work was supported by the project DEDICATE (Principal Scientist grant) at the AIT Austrian Institute of Technology. the COST Action INTERACT, CA20120, supported by COST (European Cooperation in Science and Technology) and the Czech Science Foundation, Project No. 22-04304L, Multi-band prediction of millimeter-wave propagation effects for dynamic and fixed scenarios in rugged time varying environments.

The work of A. F. Molisch was supported by the National Science Foundation grants 1926913 and 2106602, and the California Transportation Authority under the METRANS program.

References

[1] A. F. Molisch, *Wireless Communications*. John Wiley & Sons, 2023.

[2] F. Pasic, M. Hofer, M. Mussbah, S. Caban, S. Schwarz, T. Zemen, and C. F. Mecklenbräuker, "Channel estimation for mmWave MIMO using sub-6 GHz out-of-band information," in *International Conference on Smart Applications, Communications and Networking (SmartNets)*, 2024.

[3] N. Gonzalez-Prelcic, A. Ali, V. Va, and R. W. Heath, "Millimeter-wave communication with out-of-band information," *IEEE Communications Magazine*, vol. 55, no. 12, pp. 140–146, 2017.

[4] A. Ali, N. González-Prelcic, and R. W. Heath, "Millimeter wave beam-selection using out-of-band spatial information," *IEEE Transactions on Wireless Communications*, vol. 17, no. 2, pp. 1038–1052, 2017.

[5] ——, "Estimating millimeter wave channels using out-of-band measurements," in *Information Theory and Applications Workshop (ITA)*, 2016.

[6] ——, "Spatial covariance estimation for millimeter wave hybrid systems using out-of-band information," *IEEE Transactions on Wireless Communications*, vol. 18, no. 12, pp. 5471–5485, 2019.

[7] M. S. Sim, Y.-G. Lim, S. H. Park, L. Dai, and C.-B. Chae, "Deep learning-based mmwave beam selection for 5G NR/6G with sub-6 GHz channel information: Algorithms and prototype validation," *IEEE Access*, vol. 8, pp. 51 634–51 646, 2020.

[8] M. Alrabeiah and A. Alkhateeb, "Deep learning for mmwave beam and blockage prediction using sub-6 GHz channels," *IEEE Transactions on Communications*, vol. 68, no. 9, pp. 5504–5518, 2020.

[9] P. Kyösti, P. Zhang, A. Pärssinen, K. Haneda, P. Koivumäki, and W. Fan, "On the feasibility of out-of-band spatial channel information for millimeter-wave beam search," *IEEE Transactions on Antennas and Propagation*, vol. 71, no. 5, pp. 4433–4443, 2023.

[10] F. Pasic, M. Hofer, M. Mussbah, S. Sangodoyin, S. Caban, S. Schwarz, T. Zemen, M. Rupp, A. F. Molisch, and C. F. Mecklenbräuker, "Millimeter wave MIMO channel estimation using sub-6 GHz out-of-band information," *IEEE Transactions on Communications*, 2024, submitted. [Online]. Available: https://owncloud.tuwien.ac.at/index.php/s/3YP9Uq4Dxx17HeZ

[11] D. Dupleich, A. Ebert, and R. Thomä, "Measurement-based analysis of multi-band assisted beam-forming at mmwave in industrial scenarios," in *17th European Conference on Antennas and Propagation (EuCAP)*, 2023.

[12] M. Hofer, D. Löschenbrand, F. Pasic, B. Rainer, J. Blumenstein, C. F. Mecklenbräuker, S. Sangodoyin, H. Hammoud, G. Matz, A. F. Molisch, and T. Zemen, "Similarity of wireless multiband propagation in urban vehicular-to-infrastructure scenarios," in *IEEE Annual International Symposium on Personal, Indoor and Mobile Radio Communications (PIMRC)*. Valencia, Spain: IEEE, September 2024.

[13] L. Bernadó, T. Zemen, F. Tufvesson, A. F. Molisch, and C. F. Mecklenbrauker, "Delay and Doppler spreads of nonstationary vehicular channels for safety-relevant scenarios," *IEEE Trans. Veh. Technol.*, vol. 63, no. 1, pp. 82–93, Jan. 2014.

[14] T. Zemen, J. Gomez-Ponce, A. Chandra, M. Walter, E. Aksoy, R. He, D. Matolak, M. Kim, J. ichi Takada, S. Salous, R. Valenzuela, and A. F. Molisch, "Site-specific radio channel representation for 5G and 6G," *IEEE Communications Magazine*, October 2024.

[15] M. Kim, T. Iwata, S. Sasaki, and J.-I. Takada, "Millimeter-wave radio channel characterization using multi-dimensional sub-grid CLEAN algorithm," *IEICE Transactions on Communications*, vol. 103, no. 7, pp. 767–779, 2020.

[16] M. Hofer, D. Löschenbrand, J. Blumenstein, H. Groll, S. Zelenbaba, B. Rainer, L. Bernadó, J. Vychodil, T. Mikulasek, E. Zöchmann, S. Sangodoyin, H. Hammoud, B. Schrenk, R. Langwieser, S. Pratschner, A. Prokes, A. F. Molisch, C. F. Mecklenbräuker, and T. Zemen, "Wireless vehicular multiband measurements in centimeterwave and millimeterwave bands," in *IEEE 32nd Annual International Symposium on Personal, Indoor and Mobile Radio Communications (PIMRC)*, 2021, pp. 836–841.